

Article

Novel Antimicrobial Peptide “Octoprohibitin” against Multidrug Resistant *Acinetobacter baumannii*

E. H. T. Thulshan Jayathilaka ¹, Dinusha C. Rajapaksha ¹, Chamilani Nikapitiya ¹, Joeun Lee ², Mahanama De Zoysa ^{1,*} and Ilson Whang ^{2,*}

¹ College of Veterinary Medicine and Research Institute of Veterinary Medicine, Chungnam National University, Yuseong-gu, Daejeon 34134, Korea; thimira.thulshan@o.cnu.ac.kr (E.H.T.T.); dinusharajapaksha@o.cnu.ac.kr (D.C.R.); chamilani14@cnu.ac.kr (C.N.)

² National Marine Biodiversity Institute of Korea (MABIK), 75, Jangsan-ro, 101beon-gil, Janghang-eup 33662, Korea; le408@mabik.re.kr

* Correspondence: mahanama@cnu.ac.kr (M.D.Z.); ilsonwhang@mabik.re.kr (I.W.)

Abstract: Octoprohibitin is a synthetic antimicrobial peptide (AMP), derived from the prohibitin-2 gene of *Octopus minor*. It showed substantial activity against multidrug resistant (MDR) *Acinetobacter baumannii* with a minimum inhibitory concentration (MIC) and minimum bactericidal concentration (MBC) of 200 and 400 µg/mL, respectively. Time-kill kinetics and bacterial viability assays confirmed the concentration-dependent antibacterial activity of octoprohibitin against *A. baumannii*. The morphology and ultrastructure of *A. baumannii* were altered by treatment with octoprohibitin at the MIC and MBC levels. Furthermore, propidium iodide-fluorescein diacetate (PI-FDA) staining and 2',7'-dichlorodihydrofluorescein diacetate (H₂DCFDA) staining of octoprohibitin-treated *A. baumannii* revealed membrane permeability alterations and reactive oxygen species (ROS) generation, respectively. Agarose gel retardation results confirmed the DNA-binding ability of octoprohibitin to the genomic DNA of *A. baumannii*. Furthermore, octoprohibitin showed concentration-dependent inhibition of biofilm formation and eradication. The minimum biofilm inhibition concentration (MBIC) and minimum biofilm eradication concentration (MBEC) of octoprohibitin were 1000 and 1460 µg/mL, respectively. Octoprohibitin produced no significant cytotoxicity up to 800 µg/mL, and no hemolysis was observed up to 400 µg/mL. Furthermore, in vivo analysis in an *A. baumannii*-infected zebrafish model confirmed the effective bactericidal activity of octoprohibitin with higher cumulative survival percent (46.6%) and fewer pathological signs. Histological analysis showed reduced alterations in the gut, kidney, and gill tissues in the octoprohibitin-treated group compared with those in the phosphate-buffered saline (PBS)-treated group. In conclusion, our results suggest that octoprohibitin is a potential antibacterial and antibiofilm agent against MDR *A. baumannii*.

Keywords: *Acinetobacter baumannii*; antimicrobial peptide; biofilm inhibition; biofilm eradication; multidrug resistance; octoprohibitin; zebrafish



Citation: Jayathilaka, E.H.T.T.; Rajapaksha, D.C.; Nikapitiya, C.; Lee, J.; De Zoysa, M.; Whang, I. Novel Antimicrobial Peptide “Octoprohibitin” against Multidrug Resistant *Acinetobacter baumannii*. *Pharmaceuticals* **2022**, *15*, 928. <https://doi.org/10.3390/ph15080928>

Academic Editor: Donatella Tondi

Received: 8 June 2022

Accepted: 22 July 2022

Published: 27 July 2022

Publisher’s Note: MDPI stays neutral with regard to jurisdictional claims in published maps and institutional affiliations.



Copyright: © 2022 by the authors. Licensee MDPI, Basel, Switzerland. This article is an open access article distributed under the terms and conditions of the Creative Commons Attribution (CC BY) license (<https://creativecommons.org/licenses/by/4.0/>).

1. Introduction

Acinetobacter baumannii is an opportunistic pathogen, associated with most hospital-derived *Acinetobacter* infections [1]. *A. baumannii* infection is frequent in immunocompromised patients with skin and soft tissue diseases, surgical sites, bloodstream infections, and urinary tract infections [2]. Aerobic, non-fermentative, Gram-negative, non-motile bacillus, *A. baumannii*, harbors multiple virulence factors to survive in a wide range of adverse conditions and persists on surfaces for a long time in an inactive form. The possession of an intrinsic efflux pump, genetic adaptation, biofilm formation, and the presence of several beta-lactamase inhibitors are the main defense mechanisms of *A. baumannii* for the development of antibiotic resistance [3]. In recent studies, *A. baumannii* was found to be resistant to multiple antibiotics, including carbapenem, which is the last line of drugs

for controlling it [4]. At present, combination antibiotic therapy is the final solution used in the medical fraternity for controlling multidrug resistant (MDR) *A. baumannii*, which makes treatment procedures more complex and has more incidences of side effects [5]. The development of alternatives to antibiotics is the only solution for overcoming the challenges of MDR *A. baumannii* [6].

Tackling antibiotic resistance has become a major challenge in the healthcare system, and thus far, multiple compounds, such as probiotics, prebiotics, organic acids, antimicrobial peptides (AMPs), nanomaterials, and bacteriophages, have been tested as possible candidates [7–9]. Most of AMPs are natural antimicrobial compounds synthesized by organisms from archaea to mammals as a group of compounds involved in innate immunity. AMPs play a key role in defending the host against pathogenic bacteria, fungi, protozoa, and viruses [10]. AMPs are diverse within and across species, sharing common features consisting of 10 to 50 amino acid (AA) residues, water solubility, and high hydrophobicity with a positive charge (majority of AMPs). Depending on their secondary structure, AMPs can be divided into α -helices, β -sheets, and extenders [11]. AMPs possess multiple modes of action, from initial membrane disruptions to DNA and RNA damage, induction of reactive oxygen species (ROS) generation, and denaturation of proteins and enzymes [12]. Since AMPs acquire multiple modes of action and are not constrained to a single pathogen species, the possibility of the development of AMP resistance by the pathogen is at the lowest possible level [13]. Moreover, the majority of newly discovered and synthesized AMPs have shown extremely low or no toxicity towards humans and other tested animals [14]. Considering the characteristics and functional features of AMPs with low toxicity, AMPs have potential for the next generation of antimicrobials.

Marine invertebrates are deficient in adaptive immunity and primarily depend on innate immunity, which consists of physical and chemical compounds, including AMPs [15]. *Octopus minor* is considered a rich source of novel AMPs, and we synthesized octominin and octopromycin in previous studies [16,17]. Octominin, which is based on defense protein-3, showed potent bactericidal and fungicidal activities against *A. baumannii* and *Candida albicans*, respectively, whereas octopromycin, which is based on proline-rich 5 protein, showed high antibacterial activity against *A. baumannii* [16–18]. Prohibitin is a highly conserved class of proteins that inhibits cellular proliferation and has other roles in nuclear signaling, mitochondrial integrity, cell division, and cellular membrane metabolism [19]. We found the prohibitin-2 gene in the *O. minor* transcriptome, which was selected for the development of octoprohibitin as a novel AMP. Initially, we tested the antibacterial activity of octoprohibitin against *A. baumannii* and its detailed modes of action, including morphological and structural changes of the surface, membrane permeability alterations, ROS, and DNA binding ability. Furthermore, we tested octoprohibitin as an antibiofilm agent by inhibition of biofilm formation and biofilm eradication assays. Ultimately, an *A. baumannii*-infected zebrafish model was used to determine in vivo efficacy of Octoprohibitin for controlling the infection.

2. Results

2.1. Designing, Synthesis, and Characterization of Octoprohibitin

The AA sequence of *O. minor* prohibitin-2 cDNA sequence was selected as a template to synthesize octoprohibitin. Octoprohibitin exhibited characteristic features of AMPs with a net positive charge of +10, a high number of positively charged residues (arginine and lysine), and a hydrophobic ratio of 38% with two hydrophobic AAs on the surface. Furthermore, octoprohibitin has a predicted aliphatic index of 63.46, a grand average hydropathicity value (GRAVY) of -1.146 , and a molecular weight of 3333.14 Da. The predicted secondary structure of the alpha-helix (helical wheel projection diagram) and tertiary (three-dimensional) structure of octoprohibitin are shown in Figure 1. The HPLC analysis results indicated that the peak for octoprohibitin was obtained at 14.98 min (Supplementary Figure S1).

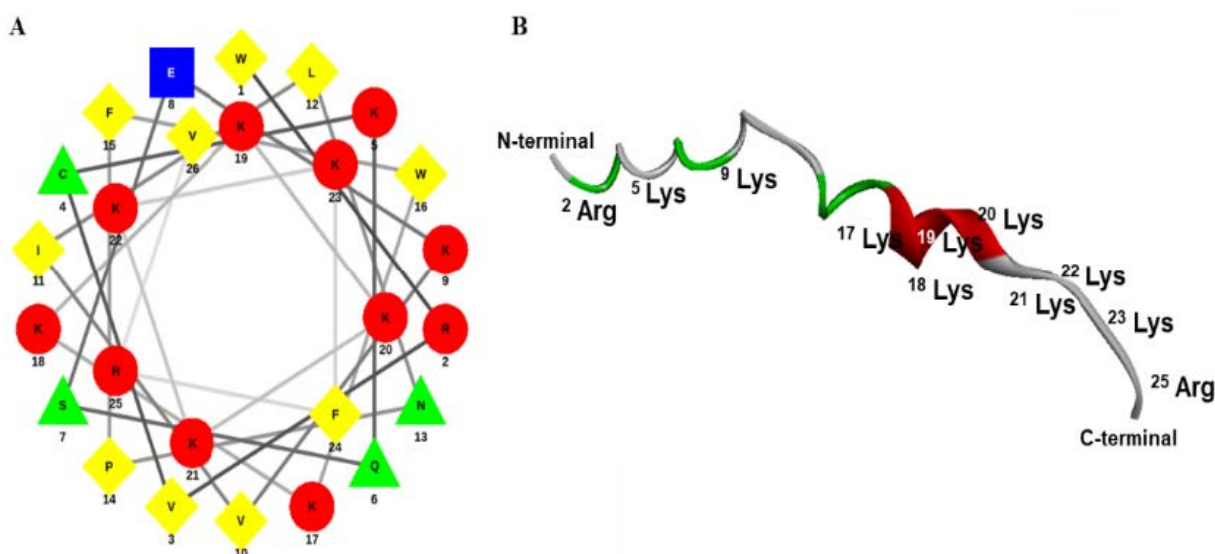


Figure 1. Octoprohibitin predicted secondary and tertiary structures. (A) Octoprohibitin helical wheel illustration. The AAs are arranged with the number of residues that are counted from the amino (N-) terminal. Basic residues and acidic residues are given in red colour circles and blue colour square, respectively, while polar and non-polar residues are demonstrated in a green colour triangle and yellow colour rhombus, respectively. (B) The tertiary structure (3D structure) of Octoprohibitin with positively charged residues are marked.

2.2. Antibacterial Activity of Octoprohibitin against *A. baumannii*

Since octoprohibitin showed relatively lower antimicrobial activity against *A. baumannii* at pH 7.4, we used the broth microdilution method at pH 7, 8, and 9 to determine the optimum pH level and found that octoprohibitin showed efficient antibacterial activity with increasing pH (Supplementary Figure S2). We selected Luria-Bertani broth (LB broth; Invitrogen, MA, USA) at pH 8 as the culture medium for further experiments because the optimum pH value for *A. baumannii* growth is 5–8 [20]. To confirm the antibacterial activity of octoprohibitin against *A. baumannii*, minimum inhibitory concentration (MIC) and minimum bactericidal concentration (MBC) were determined as 200 and 400 $\mu\text{g}/\text{mL}$, respectively, using the broth microdilution method and agar plating method. The calculated MBC/MIC ratio was 2.0. The tested positive control (chloramphenicol; 100 $\mu\text{g}/\text{mL}$) had MIC and MBC values of 50 and 100 $\mu\text{g}/\text{mL}$, respectively, against *A. baumannii*.

To investigate the antibacterial activity of octoprohibitin, time-kill kinetic and bacterial viability assays were conducted at different concentrations (0–400 $\mu\text{g}/\text{mL}$). Time-kill kinetic data showed a growth rate reduction at higher octoprohibitin treatment concentrations from 100 $\mu\text{g}/\text{mL}$, while total bacterial growth inhibition was observed at 300 $\mu\text{g}/\text{mL}$ and above (Figure 2A).

The 3-(4,5-dimethylthiazol-2-yl)-2,5-diphenyltetrazolium bromide (MTT) assay confirmed the reduced bacterial viability following octoprohibitin treatment in a concentration-dependent manner. At lower concentrations, *A. baumannii* exhibited regular growth (Figure 2B). Significant bacterial viability reduction was observed at 50 $\mu\text{g}/\text{mL}$, with a viability of 81.33% ($p \leq 0.05$), and the inhibition continued to increase at higher concentrations. At the highest tested concentration (400 $\mu\text{g}/\text{mL}$), octoprohibitin demonstrated 36.83% bacterial viability, whereas chloramphenicol (100 $\mu\text{g}/\text{mL}$) showed 9.30% viability.

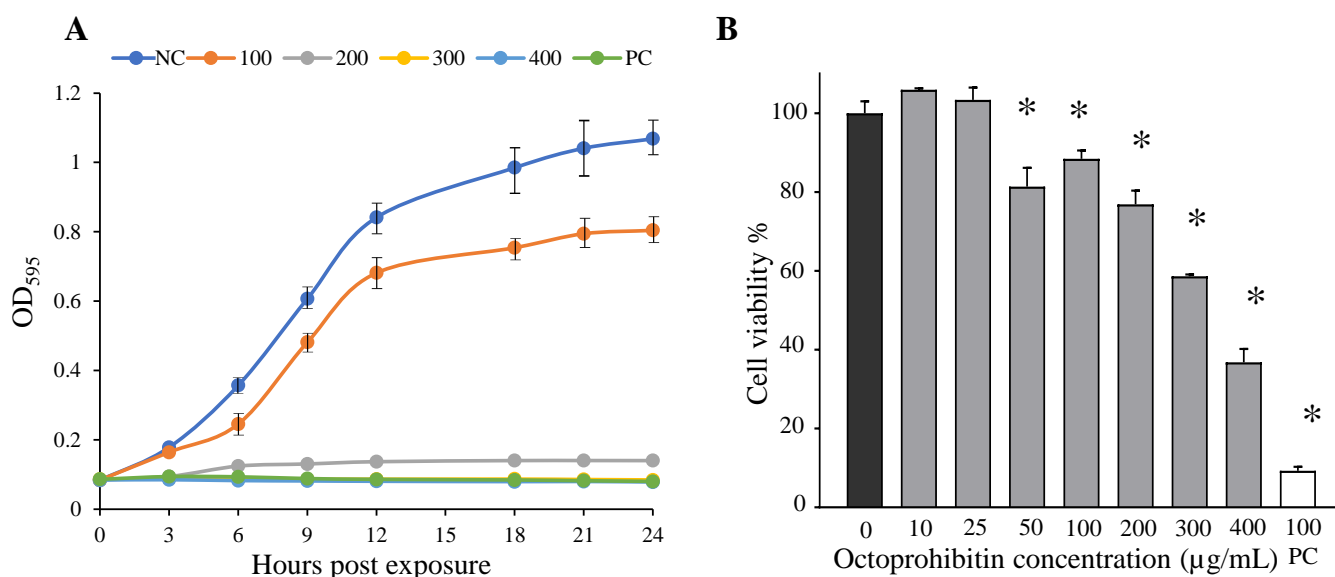


Figure 2. Octoprohibitin antibacterial activity against *A. baumannii*. (A) Time-kill kinetic of *A. baumannii*. Bacteria culture (1×10^6 CFU/mL) was treated with octoprohibitin (0, 100, 200, 300, and 400 $\mu\text{g/mL}$) and bacterial growth was observed at every 3 h time intervals at OD_{595} . As negative and positive controls, $1 \times$ phosphate buffer saline ($1 \times$ PBS) and chloramphenicol (100 $\mu\text{g/mL}$), respectively, were used. The error bars indicate the mean \pm standard deviation ($n = 3$). NC = Negative control, PC = positive control. (B) *A. baumannii* bacterial viability percentage with octoprohibitin treatment. Bacteria culture (1×10^6 CFU/mL) was treated with octoprohibitin at different concentrations (0, 10, 25, 50, 100, 200, 300, and 400 $\mu\text{g/mL}$) and chloramphenicol as positive control. MTT assay was conducted on each sample after incubation for 24 h. An unpaired two-tailed *t*-test was conducted to derive the significant differences between the negative control and the treated samples. * $p < 0.05$ compared to the control (0) group. The error bars indicate the mean \pm standard deviation ($n = 3$). PC = positive control.

2.3. Morphological and Ultrastructural Changes in *A. baumannii* with Octoprohibitin Treatment

Field-emission scanning electron microscopy (FE-SEM) was conducted to examine the effect of octoprohibitin on the morphology and ultrastructure of *A. baumannii*. Micrographs of FE-SEM analysis revealed considerable damage to the *A. baumannii* cell surface at octoprohibitin MIC (200 $\mu\text{g/mL}$) and MBC (400 $\mu\text{g/mL}$) treatment, while bacteria in the negative control showed normal cell surface and shape (Figure 3). Furthermore, octoprohibitin-treated MBC showed prominent and more severe damage with open holes and cell shrinkage compared to that of the MIC-treated group; the damage was relatively identical to that of the positive control, chloramphenicol (100 $\mu\text{g/mL}$)-treated *A. baumannii* cells.

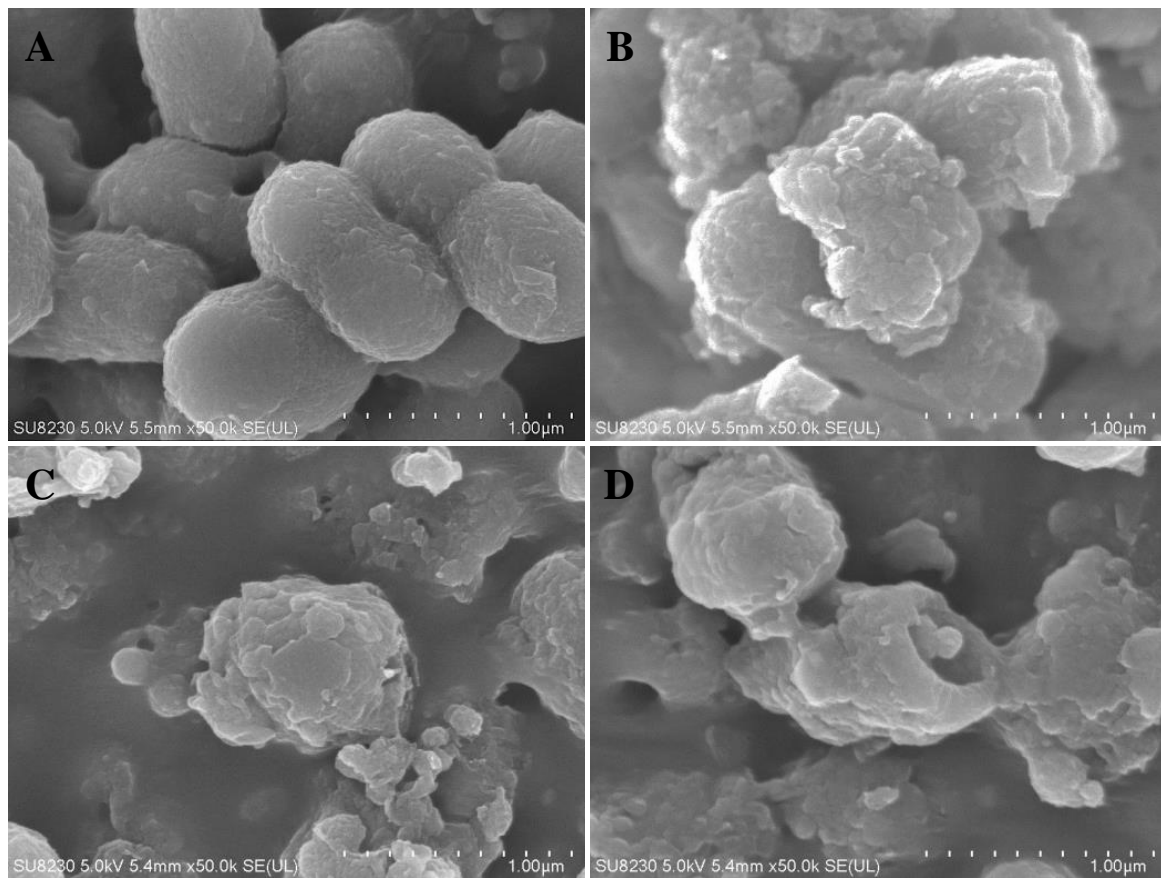


Figure 3. Morphological and structural changes of *A. baumannii* with octoprophibitin treatment. FE-SEM analysis of *A. baumannii* which were treated for 10 h with (A) PBS as a negative control, (B) MIC (200 µg/mL), (C) MBC (400 µg/mL) of octoprophibitin, and (D) chloramphenicol (100 µg/mL) as a positive control. Significant morphological and structural damages on *A. baumannii* cell surface with octoprophibitin treatment at MIC and total cell disruption at MBC were observed.

2.4. Membrane Permeability Alteration of *A. baumannii* with Octoprophibitin Treatment

With the confirmation of bacterial surface morphology alterations, a propidium iodide (PI) uptake assay was conducted to determine membrane permeability alteration in *A. baumannii* with octoprophibitin treatment. Fluorescence intensity was measured by flow cytometry (FCM), and micrographs were captured by confocal microscopy (CFMC). PI can only cross the cell membrane when permeability is altered, bind to DNA, and produce red fluorescence [21]. As expected, only the negative control (1 × PBS treated) showed red fluorescence (0.9%) compared to that of the blank (Figure 4A). Octoprophibitin treatment at MIC (200 µg/mL) and MBC (400 µg/mL) resulted in a high number of PI-stained cells with intensities of 14,689 and 18,557, respectively. Notably, chloramphenicol (100 µg/mL)-treated bacterial cells showed a fluorescence level of 14351. FCM analysis data were further confirmed using the micrographs of CFMC analysis with fluorescein diacetate (FDA) staining. FDA is permeable to live cells, and viable cells convert FDA into the green fluorescent metabolite fluorescein [22]. All the bacterial cells in the negative control showed green fluorescence (FDA-stained). Octoprophibitin at MIC, MBC and the positive control groups had prominent red fluorescein (PI-stained) cells, while a slight amount of green fluorescence cells were observed in the MIC-treated group (Figure 4B). These data suggest that octoprophibitin induces alterations in bacterial membrane permeability in *A. baumannii* in a concentration-dependent manner.

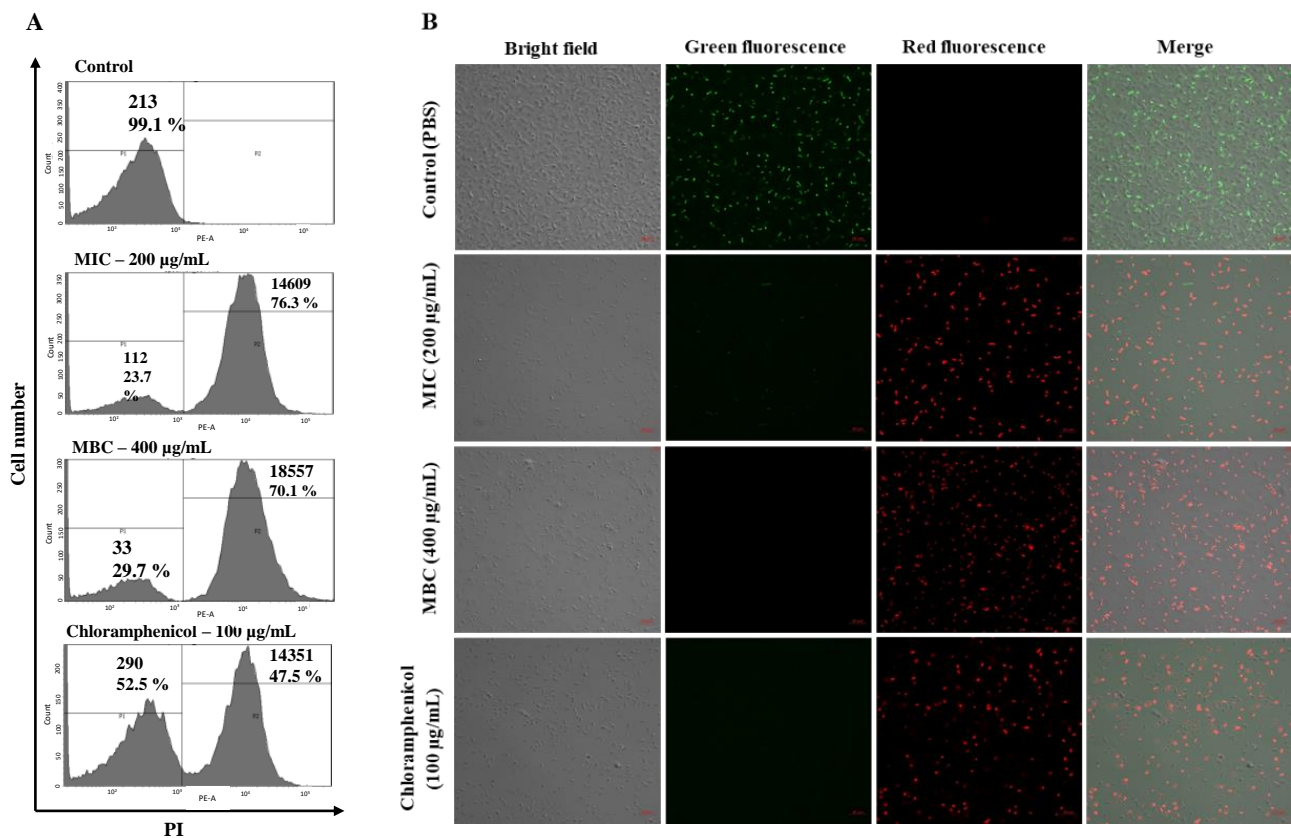


Figure 4. *A. baumannii* membrane permeability alteration with octoprohibitin treatments. (A) Flow cytometry analysis and (B) CLSM analysis on *A. baumannii* with octoprohibitin treatments at MIC (200 µg/mL), MBC (400 µg/mL), and chloramphenicol (100 µg/mL) as the positive control. Negative control was treated with 1 × PBS. After 10 h incubation, bacteria cells were stained with PI for membrane permeability altered cells and conducted flow cytometry analysis. PI- and FDA-stained cells were observed by CLSM and captured micrographs for red fluorescence (excitation—535 nm and emission—617 nm) and green fluorescence (excitation—488 nm and emission—535 nm). Scale bar; 10 µm.

2.5. Induction of ROS Generation with Octoprohibitin Treatment in *A. baumannii*

To determine ROS generation following octoprohibitin treatment, FCM and CFMC analyses were conducted on octoprohibitin-treated *A. baumannii* with 2',7'-dichlorodihydro fluorescein diacetate (H₂DCFDA) staining. Flow cytometry analysis of *A. baumannii* treated at MIC (200 µg/mL) and MBC (400 µg/mL) showed higher green fluorescence levels with 4.99- and 8.51-fold compared to that of the negative control, respectively, and the chloramphenicol (100 µg/mL)-treated group only had 4.46-fold (Figure 5A). Moreover, CFMC analysis micrographs showed a high number of green fluorescent cells in the octoprohibitin-treated groups, while the MBC group had a relatively higher number of green fluorescent cells compared to the MIC-treated group (Figure 5B). The negative control group had no green fluorescent cells, while the highest number of green fluorescent cells was observed in the positive control group. These FCM and CFMC data confirmed octoprohibitin-induced ROS generation in *A. baumannii*.

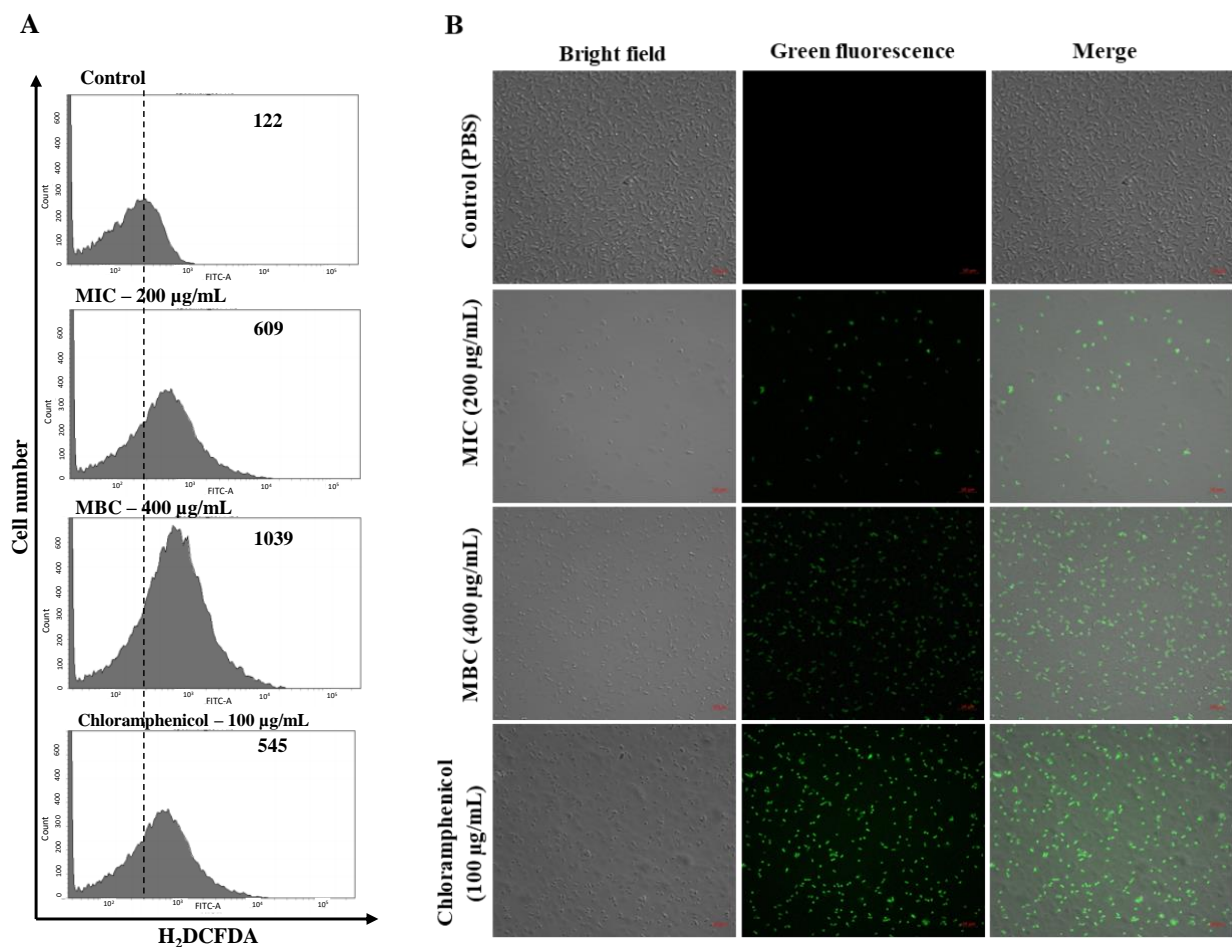


Figure 5. ROS generation of *A. baumannii* with octoprohibitin treatment. (A) Flow cytometry analysis for the fluorescence level intensity determination and (B) CLSM images of green fluorescence-stained cells for ROS production in *A. baumannii* at MIC (200 µg/mL) and MBC (400 µg/mL) treatments of octoprohibitin compared to that of the negative control (1 × PBS treated) and the positive control (chloramphenicol; 100 µg/mL treated). Bacteria cells at different treatments were stained with H₂DCFDA and observed at an excitation and emission wavelength of 488 and 535 nm, respectively.

2.6. DNA Binding Ability of Octoprohibitin with Genomic DNA of *A. baumannii*

Agarose gel retardation assay was conducted on the genomic DNA of *A. baumannii* treated with octoprohibitin to determine the DNA binding ability of octoprohibitin. Samples of genomic DNA treated with low concentrations of octoprohibitin did not exhibit significant deviation in degradation from the untreated sample (Figure 6A). However, when the treatment concentration was increased, the intensity of the DNA band decreased in a concentration-dependent manner. The lowest visible band was observed at an octoprohibitin: DNA ratio of 5:1. The DNA-binding ability of octoprohibitin was confirmed at higher ratios of octoprohibitin (7.5:1) treatments, with inhibition of genomic DNA migration and possible DNA digestion with smear appearance at those treatment levels (Figure 6B).

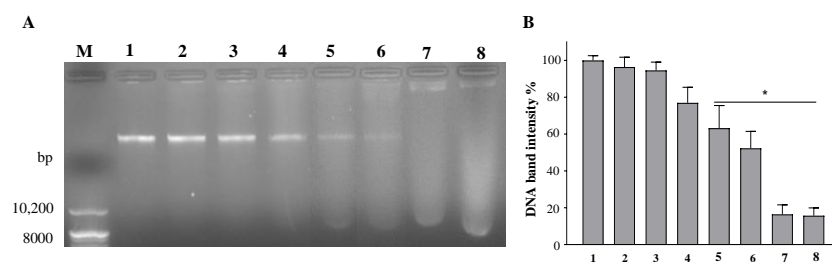


Figure 6. Agarose gel retardation assay of octoprophibitin-treated *A. baumannii* genomic DNA. Genomic DNA was reacted with octoprophibitin at different ratios ((1) 0:1, (2) 0.25:1, (3) 0.5:1, (4) 1:1, (5) 2.5:1, (6) 5:1, (7) 7.5:1, and (8) 10:1) and incubated at 37 °C for 4 h. **(A)** Total sample mixture was electroporated in 1% agarose gel. The binding ability of octoprophibitin with genomic DNA was assessed by the migration pattern of DNA. At 7.5:1 and above ratios of octoprophibitin, DNA migration was inhibited and smear formation was observed in higher concentrations of octoprophibitin. (M) DNA marker. **(B)** Quantification of DNA band intensities compared to that of the non-treated DNA sample band. An unpaired two-tailed *t*-test was conducted to derive the significant differences between the negative control and the treated samples. * $p < 0.05$ compared to the control (0) group. The error bars indicate the mean \pm standard deviation ($n = 3$).

2.7. Biofilm Formation Inhibition and Eradication Effect of Octoprophibitin on *A. baumannii*

To quantify the remaining biofilm after octoprophibitin treatment, crystal violet (CV) staining was used in biofilm formation and biofilm eradication assays. Biofilm formation was inhibited in a concentration-dependent manner, with significant ($p \leq 0.05$) inhibition observed at 25 $\mu\text{g}/\text{mL}$ (21.58%) and above (Figure 7A). The highest biofilm formation inhibition was observed at the highest tested concentration of 800 $\mu\text{g}/\text{mL}$ (91.55%). The positive control chloramphenicol (100 $\mu\text{g}/\text{mL}$) treatment group showed an 87.53% inhibition of biofilm formation. The calculated minimum biofilm inhibitory concentration (MBIC) of octoprophibitin was 1000 $\mu\text{g}/\text{mL}$. The biofilm eradication assay showed a similar pattern of concentration-dependent biofilm eradication (Figure 7B). At the highest tested concentration (800 $\mu\text{g}/\text{mL}$), a significant ($p \leq 0.05$) biofilm eradication percentage (92.11%) was observed, whereas the positive control, chloramphenicol (100 $\mu\text{g}/\text{mL}$), had 92.34% eradication. The calculated minimum biofilm eradication concentration (MBEC) for octoprophibitin was 1460 $\mu\text{g}/\text{mL}$.

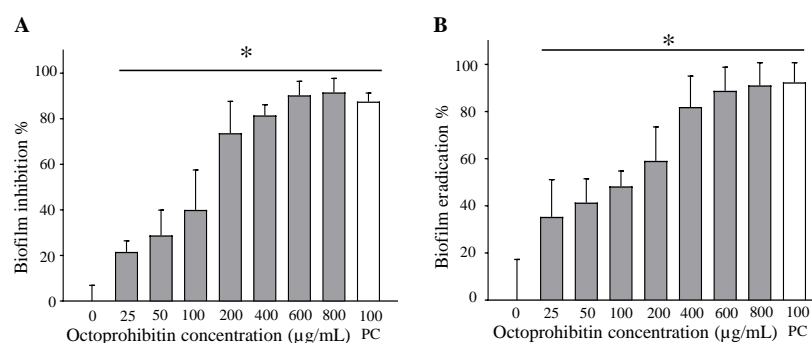


Figure 7. Antibiofilm effect of octoprophibitin against *A. baumannii* biofilm. **(A)** Biofilm formation inhibition with octoprophibitin treatment on *A. baumannii*. The bacterial culture was treated with octoprophibitin (0–800 $\mu\text{g}/\text{mL}$) and incubated for 24 h to form the biofilm. The remained biofilm after 24 h was stained by CV and quantified by absorbance measurement at OD_{595} **(B)** Biofilm eradication capacity of octoprophibitin on pre-formed *A. baumannii* biofilm. Bacteria were allowed to grow for the formation of the biofilm and treated with octoprophibitin (0–800 $\mu\text{g}/\text{mL}$). After 24 h incubation, remained biofilm was stained with CV and quantified by absorbance at OD_{595} . Data are presented as the mean \pm standard error ($n = 3$). An unpaired two-tailed *t*-test was conducted to derive the significant differences between the negative control and the treated (25–800 $\mu\text{g}/\text{mL}$) groups. * $p < 0.05$.

2.8. Hematotoxicity and Cytotoxicity of Octoprophibitin

Hemolysis assays on mouse red blood cells (RBCs) and cell viability assays on human embryonic kidney 293T (HEK293T) cells were conducted to determine the toxicity of octoprophibitin. Almost zero hemolysis was observed at octoprophibitin concentrations up to 400 µg/mL (Figure 8A). Detectable hemolysis was observed at 600 µg/mL of octoprophibitin with 26.89% of hemolysis and at 800 µg/mL, octoprophibitin showed 92.35% of hemolysis compared to that of the 100% of hemolysis in Triton x-100-treated group. In the cell viability test, a slight reduction in cell viability was observed with increasing concentrations; however, it was not significant up to 800 µg/mL. At octoprophibitin 1000 µg/mL, a significant ($p \leq 0.05$) reduction in bacterial viability (54.61%) was observed (Figure 8B).

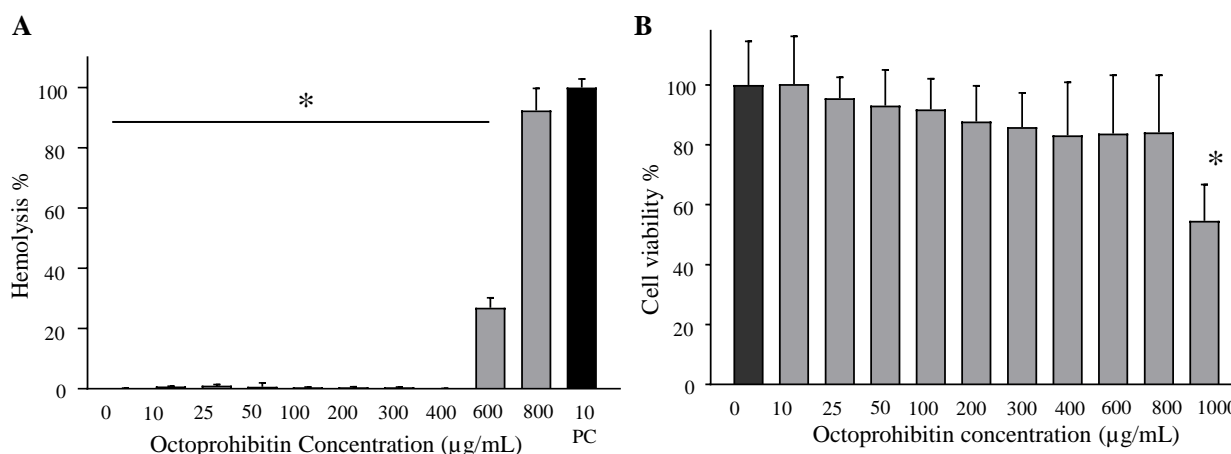


Figure 8. Hematotoxicity and cytotoxicity of octoprophibitin. (A) Hemolytic activity with octoprophibitin treatment on mouse RBCs. Washed RBCs were treated with octoprophibitin (0–800 µg/mL), 1 × PBS as the negative control, and Triton-X (10 µg/mL) as the positive control for 100% hemolysis. After 1 h incubation, RBCs were centrifuged, and the supernatant was separated for absorbance measurement at 490 nm. No hemolysis was observed up to 400 µg/mL of octoprophibitin. * $p < 0.05$ compared to the positive control (Triton-X 10 µg/mL) group. Bars indicate the mean \pm standard deviation ($n = 3$). (B) MTT assay on octoprophibitin (0–1000 µg/mL)-treated HEK 293T cells (2.0×10^5 cells/mL). No significant cell viability changes were observed in cells treated with octoprophibitin up to 800 µg/mL, * $p < 0.05$ compared to the negative control group. The error bars indicate the mean \pm standard deviation ($n = 3$).

2.9. In Vivo Effectiveness of Octoprophibitin in *A. baumannii*-Infected Zebrafish

To determine the antibacterial activity of octoprophibitin *in vivo*, adult zebrafish were challenged with *A. baumannii* and treated with octoprophibitin and tested for cumulative survival percentage (CS%), pathological signs, and histological analysis. Zebrafish that were infected and treated with PBS had the highest mortality, and the CS% at 48 h post treatment (hpt) was 13.33%. Fish that were challenged and the octoprophibitin-treated group had significantly ($p \leq 0.05$) higher CS (46.66%) than those in the PBS-treated group (Figure 9A). No mortality was observed in the negative control group throughout the experiment.

A. baumannii-infected and PBS-treated zebrafish showed pathological signs of red coloration in the abdomen area and gill area, while those signs were relatively lower in the octoprophibitin-treated group (Figure 9B). No pathological signs were observed in the negative group.

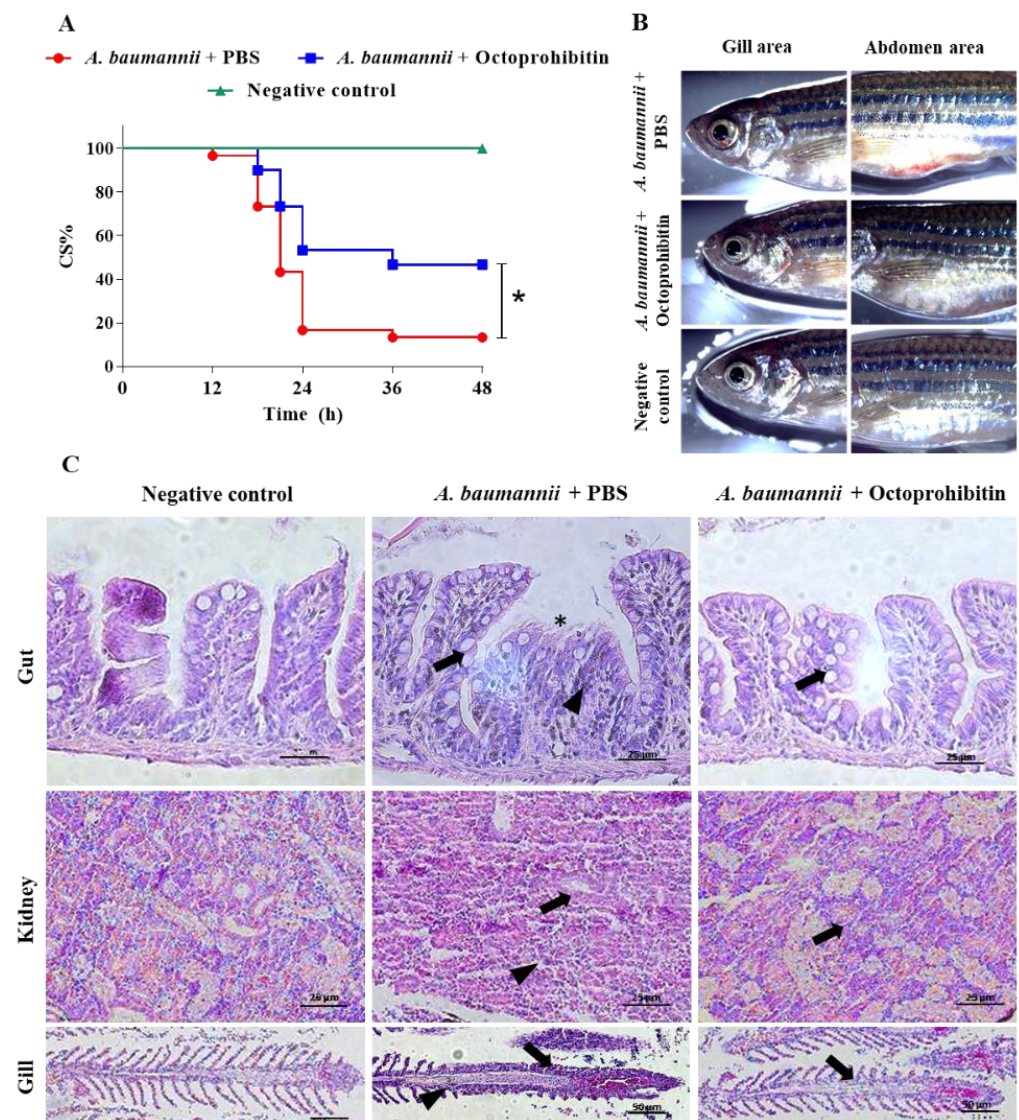


Figure 9. In vivo efficacy of octoprophibitin for controlling *A. baumannii* infection in the adult zebrafish model. (A) CS% of the adult zebrafish for 48 hpt. Zebrafish were challenged with *A. baumannii* intraperitoneally and treated with octoprophibitin or PBS. Negative control group was injected with PBS without *A. baumannii* challenge (B) Pathological signs of survived fish at 48 hpt in gill and abdomen area. (C) Histopathological analysis of gut, kidney, and gill tissues of negative control, *A. baumannii*-infected and PBS-treated and octoprophibitin treatment groups. Hyperplasia of goblet cells in gut tissue was shown in black arrow, erythrocyte infiltrations were shown in arrowhead, and epithelial damages were shown in asterisk. In kidney tissue, tubule infiltrations were shown in black arrow and tissue necrosis with low cell density was illustrated in arrowhead. In gill tissue, clubbing and shortening of secondary lamella were displayed in black arrow and thickening of primary lamella epithelial cells was shown in arrowhead.

Histological analysis showed a significant deviation in the tissue structure of the PBS-treated zebrafish group compared with that of the negative control in the gut, kidney, and gill samples (Figure 9C). Specifically, the PBS-treated group showed hyperplasia in goblet cells and erythrocyte infiltration, with epithelial cell damage in the gut tissue sample. A relatively low number of goblet cells was observed in the octoprophibitin-treated gut sample, with the absence of erythrocyte infiltration and damage to the surface epithelial cells. Kidney tissues of the PBS-treated samples showed shrinkage in the glomerulus and infiltration of proximal and distal tubules with a low density of cells due to possible tissue

necrosis. The octoprohibitin-treated sample showed minimal alterations from the negative control, with a regular tissue structure in the kidney. Clubbing and shortening of the secondary lamella and thickening of the primary lamella epithelium owing to hyperplasia were observed in the gill tissue samples of the PBS-treated zebrafish group. Tissue deformation was at a minimum level in octoprohibitin-treated gill tissue samples, and only slight thickening of the primary lamella epithelial cell layer was observed compared to that of the negative control.

3. Discussion

AMPs may be a one of major solutions for the control of MDR pathogens such as *A. baumannii*, since they contain multiple modes of action, are effective against a wide range of pathogenic species, are able to improve host immunity, and have low toxicity [23]. Marine invertebrates are rich in several AMPs because they rely mainly on innate immunity. In several previous studies, we studied *O. minor* for its AMPs and synthesized octominin and octopromycin, which showed potent antimicrobial activities against both fungi and bacteria [16,17]. In the present study, the AA sequence of the prohibitin-2 cDNA sequence was selected as a template for designing and synthesizing a novel AMP named octoprohibitin. The *A. baumannii* strain used in this study was screened for antibiotic sensitivity and was found to be resistant to multiple antibiotics in our previous study [24]. Initially, octoprohibitin showed slight antimicrobial activity against *A. baumannii* at a pH of 7.4. Some AMPs exhibit pH-dependent antimicrobial activity. Esculentin-2EM, an alpha-helical peptide isolated from *Glandirana emeljanovi*, showed a higher rate of antimicrobial activity against Gram-positive and Gram-negative bacteria at pH 8 than that at pH 6 [24]. We examined the optimum pH for the highest antibacterial activity of octoprohibitin and found more efficient bactericidal activity at pH 8 and 9. Since the optimum pH range for *A. baumannii* growth is 5–8, we selected pH 8 for *A. baumannii* culturing for further experiments with octoprohibitin treatments [25]. Potent antimicrobial activity of octoprohibitin was detected at MIC and MBC values of 200 and 400 µg/mL, respectively. The bactericidal or bacteriostatic activity of the antimicrobial agent is determined by the MBC/MIC ratio, and a compound is considered bactericidal if the ratio is below 4.0, and bacteriostatic if the ratio is higher than 4.0 [26]. Octoprohibitin is considered bactericidal rather than bacteriostatic because of its MBC/MIC ratio of 2.0. Moreover, a time-kill kinetic assay and bacterial viability test verified concentration-dependent antibacterial activity, similar to our previous finding with octominin and octopromycin against *A. baumannii* [17,18].

Cationic AMPs mainly act by disrupting the bacterial membrane. The positive charge of AMPs facilitates efficient binding to the negatively charged bacterial membrane and completes the activity through different models, such as forming pores and ion channels to induce overflow of bacterial content (barrel stave model) or disintegrating the cell membrane by changing the surface tension (carpet model) [27]. Since octoprohibitin possesses a +10 charge and amphiphilic nature, the main predicted mode of action against *A. baumannii* is morphological and structural damage to the bacterial surface and membrane permeability alterations. Micrographs of FE-SEM analysis confirmed that the surface morphology of the bacteria was altered by the formation of pores on the membrane and significant damage to the surface by octoprohibitin treatment. In addition, Mwangi et al. suggested that cathelicidin-based AMP ZY4 induces permeabilization of the *A. baumannii* membrane with a similar pattern of damage by examining the cell surface using FE-SEM [28]. According to the toroidal-pore model, cationic AMPs aggregate inside the cell membrane and alter the phospholipid monolayer of bacteria to produce nanoscale pores, which facilitates permeability alterations [29]. A PI uptake assay of octoprohibitin-treated *A. baumannii* confirmed a significant amount of membrane permeability alterations similar to the activity of octominin to induce membrane perturbation in *A. baumannii* [18]. Morphological alterations with pore formation and membrane permeability changes together might result in the leakage of the intracellular content of *A. baumannii* to the outside and cause cellular apoptosis or necrosis, ultimately causing bacterial death.

Several studies have shown that AMPs can penetrate the bacterial cell cytoplasm and induce further bactericidal activities by interrupting biochemical processes inside the cell [30]. Since octoprophobitin induces alterations in membrane surface morphology and permeability, we hypothesized that octoprophobitin could translocate into the cytoplasm and induce further antimicrobial actions. A study on LL-37, a cationic AMP, induced superoxide and peroxide production in *Escherichia coli* under aerobic conditions [31]. Increased ROS inside bacterial cells induces damage to proteins, lipids, and nucleotides, and this negative impact on bacteria is tolerable up to a certain level due to the activation of antioxidative stress response genes. Once an antimicrobial agent is capable of producing lethal stress with a significant amount of ROS, which is not borne by defense mechanisms, bacterial death is self-driven [32]. The latest findings suggest that generated ROS can cause eventual cell death by surging the self-amplification of ROS, even after the removal of the antimicrobial agent [33]. Flow cytometry and confocal microscopy analysis confirmed that octoprophobitin could increase the level of ROS inside *A. baumannii*, which could be a potential antimicrobial action that has not been well discussed previously with other AMPs in detail. However, further experiments are essential to determine the exact mechanism underlying ROS formation by octoprophobitin in *A. baumannii*.

Since we expected octoprophobitin translocation into *A. baumannii*, we predicted its cationic charge to facilitate possible binding to negatively charged genomic DNA for further expansion of the antimicrobial activity. Several AMPs depend on their antimicrobial activity by binding to bacterial DNA. BF2-A and BF2-C, which are buforin II-based AMPs isolated from Asian toads, can inhibit nucleic acid metabolism [34]. The ostrich-derived β -defensins ostricacin-1 (Osp-1) and ostricacin-2 (Osp-2) show antimicrobial activity by inhibiting protein synthesis and enzymatic activity as a result of their binding affinity to DNA [35]. Microcin-based B17 AMP can bind to DNA and block DNA replication by inhibiting the gyrase-DNA complex [36]. The gel retardation assay is the initial step in investigating the DNA-binding ability of an AMP. Since octoprophobitin showed concentration-dependent DNA binding and possible genomic DNA degradation in *A. baumannii*, it may contain further DNA-based antimicrobial activities. Further investigations are essential to determine the exact mechanism by which octoprophobitin binds to and disrupts the genomic DNA of *A. baumannii*.

A. baumannii has a remarkable capacity to form biofilms on a wide range of surfaces, from abiotic stainless steel to host epithelial cells, and it has been identified as one of the major factors for antibiotic resistance [37]. Antibiofilm AMPs can act adversely at different stages of biofilm formation through various mechanisms, including downregulation of quorum sensing, killing of early-stage biofilm, and inhibition of adhesion [38]. Octoprophobitin might also have generated similar actions to inhibit the formation of *A. baumannii* biofilms with an MBIC of 1000 $\mu\text{g}/\text{mL}$. Nevertheless, eradication of pre-formed biofilms by antimicrobials is considered challenging because biofilms consist of various defense mechanisms. To date, inadequate diffusion of antibiotics, efflux mechanisms, enzyme-facilitated deactivation, heterogenic function, slow development rate or persistent cells, and biofilm phenotype adaptive mechanisms have been identified [39,40]. We hypothesized that octoprophobitin could evade these defense mechanisms because it produced a potential disruption of the pre-formed *A. baumannii* biofilm in a concentration-dependent manner. Although octoprophobitin had significant antibiofilm effects in CV staining, further experiments are essential to define the exact inhibition and eradication mechanism of *A. baumannii* and its biofilm.

AMPs are considered to possess cell selectivity by differentiating the microbial membrane structure, and act only against pathogenic microorganisms without generating toxicity against host cells [41]. Several AMPs have been tested in vitro for their efficiency in antimicrobial activity, but their application in vivo is limited because of their toxicity to eukaryotic cells, susceptibility to proteolytic degradation, and the development of allergies [42,43]. Since octoprophobitin is positively charged and hydrophobic, we projected its selectivity towards bacterial cells and lowered its interaction with eukaryotic cells for the

least toxic effects. Since the hemolysis concentration (600 µg/mL) and HEK293T viability reduction concentration (800 µg/mL) were higher than the MIC (200 µg/mL) and MBC (400 µg/mL), we confirmed the safety of octoprophibitin for application in zebrafish to determine its effectiveness in vivo against *A. baumannii* infection.

In our previous study, we developed a zebrafish model of *A. baumannii* infection and successfully tested it with octopromycin [17]. Because we could confirm the low toxicity of octoprophibitin in vitro, the zebrafish model was used to observe how octoprophibitin treatment controls *A. baumannii* infection in vivo. As expected, octoprophibitin demonstrated its antimicrobial activity in zebrafish against *A. baumannii* infection significantly ($p < 0.05$), showing high CS% compared to that of the control group. Since visible pathological signs of hemorrhage were observed in untreated fish in the gill and abdomen area, we expanded our study to determine alterations in tissue levels by histopathology analysis. Although *A. baumannii* was not well tested in the zebrafish model previously, we identified a significant level of tissue alterations in the gut, kidney, and gills. Generally, these tissues show necrosis, reduced cell volume, and possible hemorrhages. In particular, hyperplasia of goblet cells in the gut tissue and hyperplasia and clubbing of secondary lamella in the gill confirmed the inflammatory conditions caused by *A. baumannii* in the PBS-treated control group. However, the low level of tissue damage in the octoprophibitin-treated group was confirmed by the survival data and suggested a high level of control zebrafish from *A. baumannii* infection. IDR-1, which is a derivative of bovine bactenecin, does not possess direct antimicrobial properties in vitro but was found to be protective in several mouse models infected with Gram-negative and Gram-positive pathogenic bacteria [44]. Likewise, some AMPs exhibit immunomodulatory actions in the host, such as altered chemokine and cytokine release, leukocyte activation, mast cell degranulation, anti-endotoxin generation, and chemotaxis strengthening immunity [45]. As octoprophibitin was able to control *A. baumannii* infection in zebrafish, we can conclude that protection is either by directly killing the bacteria or indirectly modulating the immunity of the host, and/or by both actions. Further experiments are essential to determine the exact mode of action of octoprophibitin in controlling *A. baumannii* infection in vivo.

Even though we have tested octoprophibitin antibacterial activity against Gram-negative *A. baumannii*, owing to its vast mode of action, such as membrane permeabilization, ROS generation, DNA binding, and antibiofilm activities, octoprophibitin may produce antibacterial activities against other Gram-negative and Gram-positive bacteria, antiviral activities, and antifungal activities. Additionally, owing to the ROS generation properties of octoprophibitin, it may be developed as an anticancer drug. However, further studies on octoprophibitin are essential for elaborating its applications in other fields.

4. Materials and Methods

4.1. Design, Synthesis, and Characterization of Octoprophibitin

The transcriptome database of *O. minor* was screened for AMPs, and the prohibitin-2 cDNA sequence was considered a candidate for designing a novel AMP. The prohibitin-2 cDNA sequence was submitted to the National Center for Biotechnology Information (NCBI) (<https://www.ncbi.nlm.nih.gov/>, accessed on 7 January 2022) database with accession number MW939430. To design octoprophibitin, the C-terminal region of the prohibitin-2 AA sequence was selected as a template. The novel AMP, octoprophibitin (WRVCKQSEKVVILNPFWKKKKKKKFRV), which contains 26 AA residues, was synthesized by a solid-phase peptide synthesis technique (AnyGen Co., Gwangju, Korea), and purified by reverse-phase high-performance liquid chromatography using a SHIMADZU C18 analytical column (Shimadzu HPLC LabSolution, Kyoto, Japan). Mass analysis was conducted using linear MALDI-TOF mass spectrometry (AXIMA Assurance, MALDI-TOF; Shimadzu, Kyoto, Japan). The three-dimensional structure of octoprophibitin was generated using APPTTEST (<https://research.timmons.eu/apptest>, accessed on 7 January 2022), and the images were visualized using Discovery Studio Visualizer (Version 21.1.0.20298, Biovia, CA, USA). The

helical wheel projection of octoprophibitin was derived by Netwheel, Peptides Helical Wheel, and Net projection maker (<http://lbqp.unb.br/etWheels/>, accessed on 7 January 2022) [18].

4.2. Analysis of Octoprophibitin Antibacterial Activity against *A. baumannii*

We conducted an initial screening of octoprophibitin activity against *A. baumannii* at pH 7.4 using the broth microdilution method. Since it showed relatively lower activity, we changed the pH of the bacterial culture broth to 7, 8, and 9 and conducted the sensitivity test similarly, and found that pH 8 was the most effective pH level. All experiments were conducted in LB broth and LB agar at pH 8. The antibacterial activity of octoprophibitin was determined by time-kill kinetics, MIC, MBC, and bacterial viability using standard assays.

MIC and time-kill kinetics assays were conducted using the broth microdilution method, whereas MBC was determined using the agar plating method according to the CLSI guidelines (M07-A10). Broth microdilution was conducted on *A. baumannii* (1×10^6 colony-forming units per milliliter; CFU/mL) in a 96-well plate (200 μ L/well), and octoprophibitin was treated with different concentrations (0–500 μ g/mL). The plate was incubated at 25 °C for 24 h, and bacterial growth was evaluated at 3 h intervals by measuring the optical density at 595 nm (OD₅₉₅) using a microplate spectrophotometer (Bio-Rad, Saint Louis, USA). Growth kinetics are illustrated for each treatment level in a line graph with OD₅₉₅ vs. time. The lowest octoprophibitin concentration that did not cause any OD₅₉₅ changes for 24 h (no bacterial growth) was selected as the MIC. To determine the MBC, octoprophibitin treated at \geq MIC bacterial broths (100 μ L) from 96-well plates was spread on LB agar plates and incubated at 25 °C for 24 h. The lowest octoprophibitin concentration that did not produce colonies on the agar plate was selected as the MBC against *A. baumannii*. The same procedure was conducted using chloramphenicol (100 μ g/mL) as a positive control to determine MIC and MBC.

To determine the reduction in bacterial viability with octoprophibitin treatment, the MTT assay was conducted according to the method described by Dananjaya et al. [46] Briefly, *A. baumannii* (1×10^6 CFU/mL) was treated with octoprophibitin (0–400 μ g/mL) and incubated at 25 °C for 4 h. Bacteria were isolated by centrifugation at $1500 \times g$ for 10 min and washed with $1 \times$ PBS. The bacterial cells were then treated with 10 μ L of MTT reagent (5 μ g/mL) (Sigma Aldrich, St. Louis, MO, USA). After incubation for 30 min, 50 μ L of dimethyl sulfoxide (DMSO) was added to the mixture (Sigma Aldrich, St. Louis City, USA) to dissolve the formazan, and the absorbance was measured using a microplate spectrophotometer at OD₅₉₅.

4.3. FE-SEM Analysis for Morphological and Structural Changes in Octoprophibitin-Treated *A. baumannii*

To determine whether octoprophibitin induces morphological and ultrastructural alterations on *A. baumannii* surfaces, FE-SEM analysis was conducted as described by Jayathilaka et al. [13]. In brief, *A. baumannii* (1×10^6 CFU/mL) was treated with the MIC (200 μ g/mL) and MBC (400 μ g/mL) of octoprophibitin, $1 \times$ PBS as the negative control, and chloramphenicol (100 μ g/mL) as the positive control. After incubation at 25 °C for 9 h, the bacterial cells were collected by centrifugation at $1500 \times g$ for 10 min and washed with $1 \times$ PBS. The isolated bacterial cells were pre-fixed with 2.5% glutaraldehyde (Pharmacia, Uppsala, Sweden) for 20 min. Each sample was washed with $1 \times$ PBS and dehydrated using a series of ethanol concentrations (30, 50, 70, 80, 90, and 100%). Cells were coated with platinum using an ion sputter (E_1030, Hitachi, Japan) and observed under FE-SEM (MERLIN™, Carl Zeiss, Germany).

4.4. Analysis of Membrane Permeability Alterations and ROS Generation

Octoprophibitin-treated *A. baumannii* was subjected to PI uptake assay and H₂DCFDA staining to determine permeability alterations and ROS generation, respectively. FCM was conducted to determine the fluorescence level, and CFMC was conducted to capture stained cell images, according to a previously described method [17,46]. Briefly, *A. baumannii*

(1×10^6 CFU/mL) was treated with octoprophibitin at MIC (200 $\mu\text{g}/\text{mL}$) and MBC (400 $\mu\text{g}/\text{mL}$), $1 \times \text{PBS}$ was used as the negative control, and chloramphenicol (100 $\mu\text{g}/\text{mL}$) was used as the positive control. Bacterial cells were collected after incubation at 25 °C for 3 and 9 h for FCM and CFMC, respectively. Isolated cells were washed with $1 \times \text{PBS}$ and resuspended in 1 mL of PBS.

For PI uptake assay, cells were treated with 50 $\mu\text{g}/\text{mL}$ PI (Sigma Aldrich, Saint Louis, USA) and 40 $\mu\text{g}/\text{mL}$ FDA (Sigma Aldrich, Saint Louis, USA) at room temperature (26 ± 2 °C) for 30 min in the dark. Similarly, samples for ROS generation were stained with H_2DCFDA (50 $\mu\text{g}/\text{mL}$) (Invitrogen, Waltham, MA, USA) at room temperature for 30 min in the dark. Excess staining was removed by centrifugation and $1 \times \text{PBS}$ washing.

To determine the fluorescence level, cell samples were resuspended in 1 mL of $1 \times \text{PBS}$, and the intensity was observed using flow cytometry (FACS Calibur, Becton Dickinson, Franklin Lakes, NJ, USA). For the PI uptake assay, the red fluorescence level was measured, and the green fluorescence level was measured for ROS generation.

To capture micrographs of fluorescent cells, bacterial samples were resuspended in 50 μL of $1 \times \text{PBS}$, and 5 μL was placed on a glass slide. Fluorescent cells were observed under CFMC with a scan head integrated into an Axiovert 200 M inverted microscope (Carl Zeiss, Jena, Germany). The red fluorescence of PI was observed at excitation and emission wavelengths of 535 and 617 nm, respectively. Green fluorescence of FDA and H_2DCFDA was observed at the excitation and emission wavelengths of 488 and 535 nm, respectively.

4.5. Agarose Gel Retardation Assay for DNA Binding Affinity

Octoprophibitin-treated genomic DNA of *A. baumannii* was subjected to an agarose gel retardation assay to determine the DNA-binding ability according to the method described by Jayathilaka et al. [18]. Genomic DNA was isolated from *A. baumannii* according to the manufacturer's protocol using an AccuPrep[®] Genomic DNA Extraction Kit (Bioneer, Daejeon, South Korea). Isolated DNA was quantified using a NanoDrop One^C Microvolume UV-Vis spectrophotometer (Thermo Scientific[™], Waltham, MA, USA). Octoprophibitin treatment was performed on 200 ng of genomic DNA at increasing ratios (0:1, 0.25:1, 0.5:1, 1:1, 2.5:1, 5:1, 7.5:1, and 10:1) and incubated at 37 °C for 4 h. The total amount of DNA was loaded onto a 1% agarose gel with 2 μL of loading buffer (Takara Bio Inc. Kusatsu, Shiga, Japan) and electroporated in a mini-submarine electrophoresis system (Mupid[®]-2plus, Takara Bio Inc. Kusatsu, Shiga, Japan) for 40 min. A photograph of the gel was captured using a gel imaging system (MaXidoc[™] G2, DAIHAN[®], Republic of Korea). The intensity of each gel band was quantified using ImageJ software (ImageJ, ver. 1.6, Rasband, WS, USA), and normalized to the intensity of the untreated gel band.

4.6. Biofilm Inhibition and Eradication Activity Assay of Octoprophibitin

Biofilm formation inhibition and eradication assays were conducted on *A. baumannii* planktonic and its biofilm, respectively, with CV staining according to the method described by Kim et al. [47]. *A. baumannii* was cultured in LB broth (pH 8) supplemented with 0.1% glucose to enhance and stabilize biofilm formation. For the biofilm inhibition assay, *A. baumannii* (1×10^6 CFU/mL) broth was added to a 96-well plate (100 $\mu\text{L}/\text{well}$), treated with octoprophibitin at different concentrations (0–1000 $\mu\text{g}/\text{mL}$) and chloramphenicol (100 $\mu\text{g}/\text{mL}$) as a positive control, and incubated for 24 h. For the biofilm eradication assay, initially, *A. baumannii* (1×10^6 CFU/mL) broth (100 $\mu\text{L}/\text{well}$) was added and allowed to form biofilms on the wall of the 96-well plate. After biofilm formation with 24 h incubation at 25 °C, the supernatant was removed and replaced with fresh media. Octoprophibitin (0–800 $\mu\text{g}/\text{mL}$) or chloramphenicol (100 $\mu\text{g}/\text{mL}$) was added to the biofilm and incubated for 24 h at 25 °C.

After octoprophibitin treatment, the biofilm formation inhibition and biofilm eradication assay plates were used for CV staining. The supernatant was removed, and the wells were washed with $1 \times \text{PBS}$ to remove planktonic bacteria. Absolute methanol (100 $\mu\text{L}/\text{well}$) was used to fix the biofilms for 10 min. After removal of methanol, 100 μL of 0.1% CV (Sigma-

Aldrich, Burlington, MA, USA) was used to stain the biofilm at room temperature for 30 min. The CV was then removed, and the wells were washed with $1 \times$ PBS to remove unbound CV. Biofilm-bound CV was dissolved by adding absolute ethanol (100 μ L/well) and mixing. The absorbance of each well was measured using a microplate spectrophotometer at OD₅₉₅. The biofilm formation inhibition and eradication percentages were calculated. Biofilm formation inhibition/eradication % = $[1 - (Ab_{\text{test}}/Ab_{\text{negative control}})] \times 100\%$, where Ab_{test} represents the absorbance value of octoprophibitin or chloramphenicol; $Ab_{\text{negative control}}$ represents the absorbance of the negative control (PBS). Ninety percent of the biofilm formation inhibition concentration and eradication concentration were calculated as MBIC and MBEC, respectively.

4.7. Hemolysis Assay and Cytotoxicity Assay for Determination of Octoprophibitin Toxicity

To determine the toxicity level of octoprophibitin, a hemolysis assay on mouse RBCs and a cytotoxicity test on HEK293T cells (American Type Culture Collection ATCC-11268) were conducted. For the hemolysis assay, RBCs were collected by centrifuging mouse blood at $1500 \times g$ and washed with $1 \times$ PBS. Then, RBCs were suspended in $1 \times$ PBS and treated with octoprophibitin at different concentrations (0–800 μ g/mL), with $1 \times$ PBS as the negative control and 1% (w/v) Triton x-100 (Sigma Aldrich, Saint Louis, MO, USA) as the positive control. After incubation at 37 °C for 4 h, the supernatant was separated by centrifugation at $1500 \times g$ and the absorbance was measured using a microplate spectrophotometer at 490 nm. The hemolysis percentage was calculated by normalizing with the 100% hemolysis absorbance using 1% Triton X-100. Hemolysis (%) = $((Ab_{\text{test}} - Ab_{\text{PBS}})/(Ab_{\text{triton}} - Ab_{\text{PBS}})) \times 100\%$, where Ab_{test} represents the absorbance of octoprophibitin-treated RBCs supernatant, Ab_{PBS} represents the absorbance of PBS-treated RBCs supernatant, and Ab_{triton} represents the absorbance of Triton X-100-treated RBCs supernatant.

An MTT assay was conducted to determine the change in viability of HEK293T cells treated with octoprophibitin. Briefly, HEK293T cells were seeded in Dulbecco's modified Eagle's medium (Invitrogen, Carlsbad, CA, USA) with 1% antibiotic/antimycotic solution (Gibco, Carlsbad, CA, USA) and 10% fetal bovine serum (Hyclone, Carlsbad, CA, USA). Then, the cells were seeded in a 96-well plate at a cell density of 1.5×10^6 cells/well and incubated at 37 °C in a 5% CO₂ atmosphere. After 24 h of incubation, the supernatant was removed and replaced with a fresh medium. Octoprophibitin treatment was conducted in a concentration series (0–800 μ g/mL) and incubated at 37 °C in a 5% CO₂ atmosphere for 24 h. Culture media was replaced with 90 μ L fresh media and 10 μ L of MTT reagent (5 μ g/mL). After incubation at 37 °C for 4 h, 50 μ L DMSO was added to each well and mixed. Solubilized formazan was quantified by absorbance measurement using a microplate spectrophotometer at OD₅₉₅.

4.8. In Vivo Octoprophibitin Efficacy Assay against *A. baumannii*-Infected Zebrafish

In vivo zebrafish experiments were performed according to the institutional animal ethics guidelines and under the supervision of the Committee of Chungnam National University (202103-CNU-072). Bacteria (*A. baumannii*) challenge and octoprophibitin treatment were conducted intraperitoneally in zebrafish according to the method described by Liyanage et al. [48]. Briefly, zebrafish were divided into three groups (30 fish per group in triplicate) and labeled; 1) only PBS-treated (negative control), 2) *A. baumannii* challenged and $1 \times$ PBS-treated, and 3) *A. baumannii* challenged and octoprophibitin-treated. First, zebrafish were anesthetized using 160 μ g/mL buffered tricaine (ethyl 3-aminobenzoate methanesulfonate; Sigma-Aldrich, USA) and injected with an infective dose of *A. baumannii* (20 μ L of 2.1×10^{11} CFU/mL). Then, treatment was conducted with either 10 μ L of octoprophibitin (10 μ g/mL) or 10 μ L of $1 \times$ PBS. The negative control group was injected with 30 μ L $1 \times$ PBS. Fish were placed in tanks and maintained at 28 °C while observing mortality every 6 h for 48 h. The pathological signs were monitored in the remaining fish at 48 hpt. Finally, CS% was calculated.

For histopathological analysis, three zebrafish per group were sacrificed for collection of gut, kidney, and gill tissues at the end of the experiment. Histological analysis was performed according to the method described by Liyanage et al. [48]. The collected tissues were processed, embedded, and sectioned to a thickness of 4 μm , and glass slides were prepared for each section. Hematoxylin and eosin staining was performed, and the slides were observed under a light microscope (Leica 3000 LED, Wetzlar, Germany).

5. Conclusions

Octoprohibitin exhibited bactericidal activity against *A. baumannii* in a concentration-dependent manner, with MIC and MBC values of 200 and 400 $\mu\text{g}/\text{mL}$, respectively. *A. baumannii* growth and viability reductions were observed with increasing concentrations of octoprohibitin. Morphological and structural changes in the bacterial surface, membrane permeability alteration, ROS generation, and DNA-binding activity were determined as possible modes of action for the efficient killing activity of *A. baumannii* and preventing the development of antimicrobial resistance. In addition to its antimicrobial activity, octoprohibitin showed concentration-dependent antibiofilm activity, with biofilm formation inhibition and biofilm eradication. The MBIC and MBEC were 1000 and 1460 $\mu\text{g}/\text{mL}$, respectively. Hemolysis and cell viability assays confirmed that the toxic concentrations of octoprohibitin are above the MIC and MBC and are safer to use in vivo experiments. Finally, we found the efficiency of octoprohibitin in controlling *A. baumannii* not only in vitro but also in vivo, with higher survival of zebrafish and least damage to the gut, kidney, and gill tissues in the zebrafish model. Further experiments can descriptively explain the actions, safety, and application of octoprohibitin, and finally, introduce it as a pharmaceutical product to control multidrug resistance in nosocomial *A. baumannii*.

Supplementary Materials: The following supporting information can be downloaded at: <https://www.mdpi.com/article/10.3390/ph15080928/s1>, Figure S1: Octoprohibitin HPLC mass spectrophotometry chromatographs; Figure S2: *A. baumannii* time-kill kinetics of octoprohibitin at pH 7, 8 and 9.

Author Contributions: E.H.T.T.J.: Methodology, Investigation, Formal analysis, Writing—original draft, Writing—review and editing. D.C.R.: Investigation and Formal analysis. J.L.: Project administration, Methodology, Writing—review and editing. C.N.: Methodology, Supervision, Writing—review and editing. M.D.Z.: Conceptualization, Funding acquisition, Methodology, Project administration, Supervision, Writing—review and editing. I.W.: Conceptualization, Funding acquisition, Project administration, Methodology, Writing—review and editing. All authors have read and agreed to the published version of the manuscript.

Funding: This work was supported by the Research Program of the National Marine Biodiversity Institute of Korea (MABIK2022M00400), funded by the Ministry of Oceans and Fisheries, and by the National Research Foundation of Korea (NRF) grant funded by the Korean government (MSIT) (2019R1A2C1087028).

Institutional Review Board Statement: Institutional animal ethics guidelines and supervision of the committees of Chungnam National University (202103-CNU-072).

Informed Consent Statement: Not applicable.

Data Availability Statement: Data is contained within the article and Supplementary Materials.

Acknowledgments: This work was supported by the Research Program of the National Marine Biodiversity Institute of Korea (MABIK2022M00400), funded by the Ministry of Oceans and Fisheries, and by the National Research Foundation of Korea (NRF) grant funded by the Korean government (MSIT) (2019R1A2C1087028).

Conflicts of Interest: The authors declare that they have no conflict of interest.

References

1. Vahdani, P.; Yaghoubi, T.; Aminzadeh, Z. Hospital acquired antibiotic-resistant *Acinetobacter baumannii* infections in a 400-bed hospital in Tehran, Iran. *Int. J. Prev. Med.* **2011**, *2*, 127. [[PubMed](#)]
2. Guerrero, D.M.; Perez, F.; Conger, N.G.; Solomkin, J.S.; Adams, M.D.; Rather, P.N.; Bonomo, R.A. *Acinetobacter baumannii*-associated skin and soft tissue infections: Recognizing a broadening spectrum of disease. *Surg. Infect.* **2010**, *11*, 49–57. [[CrossRef](#)] [[PubMed](#)]
3. Abdi, S.N.; Ghotaslou, R.; Ganbarov, K.; Mobed, A.; Tanomand, A.; Yousefi, M.; Asgharzadeh, M.; Kafil, H.S. *Acinetobacter baumannii* efflux pumps and antibiotic resistance. *Infect. Drug Resist.* **2020**, *13*, 423. [[CrossRef](#)] [[PubMed](#)]
4. Evans, B.A.; Hamouda, A.; Amyes, S.G.B. The rise of carbapenem-resistant *Acinetobacter baumannii*. *Curr. Pharm. Des.* **2013**, *19*, 223–238. [[CrossRef](#)]
5. Paul, M.; Carmeli, Y.; Durante-Mangoni, E.; Mouton, J.W.; Tacconelli, E.; Theuretzbacher, U.; Mussini, C.; Leibovici, L. Combination therapy for carbapenem-resistant Gram-negative bacteria. *J. Antimicrob. Chemother.* **2014**, *69*, 2305–2309. [[CrossRef](#)]
6. Gaur, R.K. Antibiotic resistance: Alternative approaches. *Indian J. Pharmacol.* **2017**, *49*, 208.
7. Munir, M.U.; Ahmed, A.; Usman, M.; Salman, S. Recent advances in nanotechnology-aided materials in combating microbial resistance and functioning as antibiotics substitutes. *Int. J. Nanomed.* **2020**, *15*, 7329–7358. [[CrossRef](#)]
8. Munir, M.U.; Ahmad, M.M. Nanomaterials Aiming to Tackle Antibiotic-Resistant Bacteria. *Pharmaceutics* **2022**, *14*, 582. [[CrossRef](#)] [[PubMed](#)]
9. Bush, K.; Courvalin, P.; Dantas, G.; Davies, J.; Eisenstein, B.; Huovinen, P.; Jacoby, G.A.; Kishony, R.; Kreiswirth, B.N.; Kutter, E. Tackling antibiotic resistance. *Nat. Rev. Microbiol.* **2011**, *9*, 894–896. [[CrossRef](#)]
10. Li, Y.; Xiang, Q.; Zhang, Q.; Huang, Y.; Su, Z. Overview on the recent study of antimicrobial peptides: Origins, functions, relative mechanisms and application. *Peptides* **2012**, *37*, 207–215. [[CrossRef](#)]
11. Moghaddam, M.M.; Aghamollaei, H.; Kooshki, H.; Barjini, K.A.; Mirnejad, R.; Choopani, A. The development of antimicrobial peptides as an approach to prevention of antibiotic resistance. *Rev. Med. Microbiol.* **2015**, *26*, 98–110. [[CrossRef](#)]
12. Id, M.Y.; Dutta, D.; Willcox, M.D.P. Mode of action of the antimicrobial peptide Mel4 is independent of *Staphylococcus aureus* cell membrane permeability. *PLoS ONE* **2019**, *14*, e0215703.
13. Hancock, R.E.W.; Sahl, H.-G. Antimicrobial and host-defense peptides as new anti-infective therapeutic strategies. *Nat. Biotechnol.* **2006**, *24*, 1551–1557. [[CrossRef](#)] [[PubMed](#)]
14. Javadpour, M.M.; Juban, M.M.; Lo, W.-C.J.; Bishop, S.M.; Albery, J.B.; Cowell, S.M.; Becker, C.L.; McLaughlin, M.L. De novo antimicrobial peptides with low mammalian cell toxicity. *J. Med. Chem.* **1996**, *39*, 3107–3113. [[CrossRef](#)]
15. Sperstad, S.V.; Haug, T.; Blencke, H.-M.; Styrvold, O.B.; Li, C.; Stensvåg, K. Antimicrobial peptides from marine invertebrates: Challenges and perspectives in marine antimicrobial peptide discovery. *Biotechnol. Adv.* **2011**, *29*, 519–530. [[CrossRef](#)]
16. Nikapitiya, C.; Dananjaya, S.H.S.; Chandrarathna, H.P.S.U.; de Zoysa, M.; Whang, I. Octominin: A Novel Synthetic Anticandidal Peptide Derived from Defense Protein of *Octopus minor*. *Mar. Drugs* **2020**, *18*, 56. [[CrossRef](#)] [[PubMed](#)]
17. Rajapaksha, D.C.; Jayathilaka, E.H.T.T.; Edirisinghe, S.L.; Nikapitiya, C.; Lee, J.; Whang, I.; De Zoysa, M. Octopromycin: Antibacterial and antibiofilm functions of a novel peptide derived from *Octopus minor* against multidrug-resistant *Acinetobacter baumannii*. *Fish Shellfish Immunol.* **2021**, *117*, 82–94. [[CrossRef](#)] [[PubMed](#)]
18. Thulshan Jayathilaka, E.H.T.; Rajapaksha, D.C.; Nikapitiya, C.; De Zoysa, M.; Whang, I. Antimicrobial and anti-biofilm peptide octominin for controlling multidrug-resistant *Acinetobacter baumannii*. *Int. J. Mol. Sci.* **2021**, *22*, 5353. [[CrossRef](#)] [[PubMed](#)]
19. Bavelloni, A.; Piazzini, M.; Raffini, M.; Faenza, I.; Blalock, W.L. Prohibitin 2: At a communications crossroads. *IUBMB Life* **2015**, *67*, 239–254. [[CrossRef](#)]
20. Hrenovic, J.; Durn, G.; Goic-Barisic, I.; Kovacic, A. Occurrence of an environmental *Acinetobacter baumannii* strain similar to a clinical isolate in paleosol from Croatia. *Appl. Environ. Microbiol.* **2014**, *80*, 2860–2866. [[CrossRef](#)]
21. Crowley, L.C.; Scott, A.P.; Marfell, B.J.; Boughaba, J.A.; Chojnowski, G.; Waterhouse, N.J. Measuring cell death by propidium iodide uptake and flow cytometry. *Cold Spring Harb. Protoc.* **2016**, *2016*, pdb-prot087163. [[CrossRef](#)] [[PubMed](#)]
22. Kanade, S.; Nataraj, G.; Ubale, M.; Mehta, P. Fluorescein diacetate vital staining for detecting viability of acid-fast bacilli in patients on antituberculosis treatment. *Int. J. Mycobacteriol.* **2016**, *5*, 294–298. [[CrossRef](#)] [[PubMed](#)]
23. Jaśkiewicz, M.; Neubauer, D.; Kazor, K.; Bartoszewska, S.; Kamysz, W. Antimicrobial activity of selected antimicrobial peptides against planktonic culture and biofilm of *Acinetobacter baumannii*. *Probiotics Antimicrob. Proteins* **2019**, *11*, 317–324. [[CrossRef](#)] [[PubMed](#)]
24. Malik, E.; Dennison, S.R.; Harris, F.; Phoenix, D.A. pH dependent antimicrobial peptides and proteins, their mechanisms of action and potential as therapeutic agents. *Pharmaceutics* **2016**, *9*, 67. [[CrossRef](#)] [[PubMed](#)]
25. Dekic, S.; Hrenovic, J.; Ivankovic, T.; Van Wilpe, E. Survival of ESKAPE pathogen *Acinetobacter baumannii* in water of different temperatures and pH. *Water Sci. Technol.* **2018**, *78*, 1370–1376. [[CrossRef](#)] [[PubMed](#)]
26. Mogana, R.; Adhikari, A.; Tzar, M.N.; Ramliza, R.; Wiart, C. Antibacterial activities of the extracts, fractions and isolated compounds from canarium patentinervium miq. Against bacterial clinical isolates. *BMC Complement. Med. Ther.* **2020**, *20*, 55. [[CrossRef](#)] [[PubMed](#)]
27. Lei, J.; Sun, L.; Huang, S.; Zhu, C.; Li, P.; He, J.; Mackey, V.; Coy, D.H. The antimicrobial peptides and their potential clinical applications. *Am. J. Transl. Res.* **2019**, *11*, 3919–3931. [[PubMed](#)]

28. Mwangi, J.; Yin, Y.; Wang, G.; Yang, M.; Li, Y.; Zhang, Z.; Lai, R. The antimicrobial peptide ZY4 combats multidrug-resistant *Pseudomonas aeruginosa* and *Acinetobacter baumannii* infection. *Proc. Natl. Acad. Sci. USA* **2019**, *116*, 26516–26522. [[CrossRef](#)]
29. Tuerkova, A.; Kabelka, I.; Králová, T.; Sukenik, L.; Pokorná, Š.; Hof, M.; Vácha, R. Effect of helical kink in antimicrobial peptides on membrane pore formation. *eLife* **2020**, *9*, e47946. [[CrossRef](#)]
30. Moravej, H.; Moravej, Z.; Yazdanparast, M.; Heiat, M.; Mirhosseini, A.; Moosazadeh Moghaddam, M.; Mirnejad, R. Antimicrobial peptides: Features, action, and their resistance mechanisms in bacteria. *Microb. Drug Resist.* **2018**, *24*, 747–767. [[CrossRef](#)]
31. Choi, H.; Yang, Z.; Weisshaar, J.C. Oxidative stress induced in *E. coli* by the human antimicrobial peptide LL-37. *PLoS Pathog.* **2017**, *13*, e1006481. [[CrossRef](#)] [[PubMed](#)]
32. Kim, S.Y.; Park, C.; Jang, H.J.; Kim, B.O.; Bae, H.W.; Chung, I.Y.; Kim, E.S.; Cho, Y.H. Antibacterial strategies inspired by the oxidative stress and response networks. *J. Microbiol.* **2019**, *57*, 203–212. [[CrossRef](#)] [[PubMed](#)]
33. Hong, Y.; Zeng, J.; Wang, X.; Drlica, K.; Zhao, X. Post-stress bacterial cell death mediated by reactive oxygen species. *Proc. Natl. Acad. Sci. USA* **2019**, *116*, 10064–10071. [[CrossRef](#)] [[PubMed](#)]
34. Hao, G.; Shi, Y.H.; Tang, Y.L.; Le, G.W. The intracellular mechanism of action on *Escherichia coli* of BF2-A/C, two analogues of the antimicrobial peptide Buforin 2. *J. Microbiol.* **2013**, *51*, 200–206. [[CrossRef](#)]
35. Le, C.-F.; Fang, C.-M.; Sekaran, S.D. Intracellular targeting mechanisms by antimicrobial peptides. *Antimicrob. Agents Chemother.* **2017**, *61*, e02340-16. [[CrossRef](#)]
36. Collin, F.; Thompson, R.E.; Jolliffe, K.A.; Payne, R.J.; Maxwell, A. Fragments of the bacterial toxin microcin B17 as gyrase poisons. *PLoS ONE* **2013**, *8*, e61459.
37. Colquhoun, J.M.; Rather, P.N. Insights into Mechanisms of Biofilm Formation in *Acinetobacter baumannii* and Implications for Uropathogenesis. *Front. Cell. Infect. Microbiol.* **2020**, *10*, 253. [[CrossRef](#)]
38. Chung, P.Y.; Khanum, R. Antimicrobial peptides as potential anti-biofilm agents against multidrug-resistant bacteria. *J. Microbiol. Immunol. Infect.* **2017**, *50*, 405–410. [[CrossRef](#)]
39. Yang, C.H.; Su, P.W.; Moi, S.H.; Chuang, L.Y. Biofilm formation in *Acinetobacter baumannii*: Genotype-phenotype correlation. *Molecules* **2019**, *24*, 1849. [[CrossRef](#)]
40. Hall, C.W.; Mah, T.-F. Molecular mechanisms of biofilm-based antibiotic resistance and tolerance in pathogenic bacteria. *FEMS Microbiol. Rev.* **2017**, *41*, 276–301. [[CrossRef](#)]
41. Lyu, Y.; Yang, Y.; Lyu, X.; Dong, N.; Shan, A. Antimicrobial activity, improved cell selectivity and mode of action of short PMAP-36-derived peptides against bacteria and *Candida*. *Sci. Rep.* **2016**, *6*, 27258. [[CrossRef](#)]
42. Dijksteel, G.S.; Ulrich, M.M.W.; Middelkoop, E.; Boekema, B.K.H.L. Lessons learned from clinical trials using antimicrobial peptides (AMPs). *Front. Microbiol.* **2021**, *12*, 616979. [[CrossRef](#)] [[PubMed](#)]
43. Khabbaz, H.; Karimi-Jafari, M.H.; Saboury, A.A.; BabaAli, B. Prediction of antimicrobial peptides toxicity based on their physico-chemical properties using machine learning techniques. *BMC Bioinform.* **2021**, *22*, 549. [[CrossRef](#)] [[PubMed](#)]
44. Scott, M.G.; Dullaghan, E.; Mookherjee, N.; Glavas, N.; Waldbrook, M.; Thompson, A.; Wang, A.; Lee, K.; Doria, S.; Hamill, P.; et al. An anti-infective peptide that selectively modulates the innate immune response. *Nat. Biotechnol.* **2007**, *25*, 465–472. [[CrossRef](#)]
45. Hilchie, A.L.; Wuerth, K.; Hancock, R.E.W. Immune modulation by multifaceted cationic host defense (antimicrobial) peptides. *Nat. Chem. Biol.* **2013**, *9*, 761–768. [[CrossRef](#)] [[PubMed](#)]
46. Dananjaya, S.H.S.; Udayangani, R.M.C.; Oh, C.; Nikapitiya, C.; Lee, J.; De Zoysa, M. Green synthesis, physio-chemical characterization and anti-candidal function of a biocompatible chitosan gold nanocomposite as a promising antifungal therapeutic agent. *RSC Adv.* **2017**, *7*, 9182–9193. [[CrossRef](#)]
47. Kim, M.K.; Kang, N.; Ko, S.J.; Park, J.; Park, E.; Shin, D.W.; Kim, S.H.; Lee, S.A.; Lee, J.I.; Lee, S.H.; et al. Antibacterial and antibiofilm activity and mode of action of magainin 2 against drug-resistant *Acinetobacter baumannii*. *Int. J. Mol. Sci.* **2018**, *19*, 3041. [[CrossRef](#)]
48. Liyanage, T.D.; Nikapitiya, C.; Lee, J.; De Zoysa, M. Molecular insight into regulation of miRNAs in the spleen of zebrafish (*Danio rerio*) upon pathogenic *Streptococcus parauberis* infection. *Fish Shellfish Immunol.* **2020**, *106*, 898–909. [[CrossRef](#)]